

**DEUTSCHES ELEKTRONEN-SYNCHROTRON**  
**Ein Forschungszentrum der Helmholtz-Gemeinschaft**

DESY 11-165

September 2011

**Production of transform-limited X-ray pulses  
through self-seeding at the European X-ray FEL**

Gianluca Geloni,  
*European XFEL GmbH, Hamburg*

Vitali Kocharyan and Evgeni Saldin  
*Deutsches Elektronen-Synchrotron DESY, Hamburg*

ISSN 0418-9833

**NOTKESTRASSE 85 - 22607 HAMBURG**

# Production of transform-limited X-ray pulses through self-seeding at the European X-ray FEL

Gianluca Geloni,<sup>a,1</sup> Vitali Kocharyan<sup>b</sup> and Evgeni Saldin<sup>b</sup>

<sup>a</sup>*European XFEL GmbH, Hamburg, Germany*

<sup>b</sup>*Deutsches Elektronen-Synchrotron (DESY), Hamburg, Germany*

---

## Abstract

An important goal for any advanced X-ray FEL is an option for providing Fourier-limited X-ray pulses. In this way, no monochromator is needed in the experimental hall. Self-seeding is a promising approach to significantly narrow the SASE bandwidth to produce nearly transform-limited pulses. These are important for many experiments including 3D diffraction imaging. We discuss the implementation of a single-crystal self-seeding scheme in the hard X-ray lines of the European XFEL. For this facility, transform-limited pulses are particularly valuable since they naturally support the extraction of more FEL power than at saturation by exploiting tapering in the tunable-gap baseline undulators. Tapering consists of a stepwise change of the undulator gap from segment to segment. Based on start-to-end simulations dealing with the up-to-date parameters of the European XFEL, we show that the FEL power reaches about 400 GW, or one order of magnitude higher power than the SASE saturation level (20 GW). This analysis indicates that our self-seeding scheme is not significantly affected by non-ideal electron phase-space distribution, and yields about the same performance as in the case for an electron beam with ideal parameters. The self-seeding scheme with a single crystal monochromator is extremely compact (about 5 m long), and cost estimations are low enough to consider adding it to the European XFEL capabilities from the very beginning of the operation phase.

---

## 1 Introduction

Conventional SASE X-ray FELs like the European X-ray FEL provide transversely coherent beams, but only limited longitudinal coherence [1]-[3].

---

<sup>1</sup> Corresponding Author. E-mail address: gianluca.geloni@xfel.eu

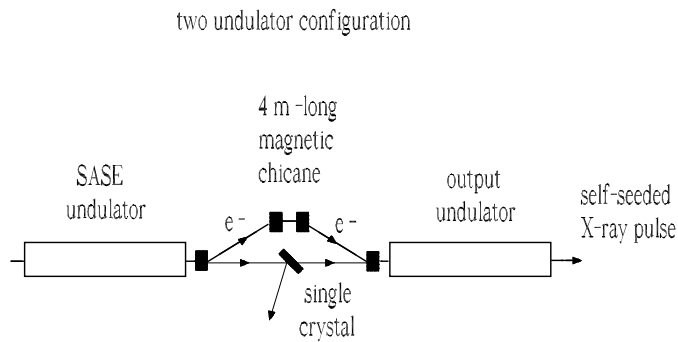


Fig. 1. Schematics of a single-crystal self-seeding scheme for hard X-rays. It will rely on a diamond crystal, C(400) reflection, in Bragg geometry.

Many experiments, including 3D diffraction imaging, require both transverse and longitudinal coherence. In principle, one can create a longitudinally coherent source by use of a monochromator located in the experimental hall, but this is often undesirable because of intensity losses. An important goal for the European X-ray FEL is the production of X-ray pulses with the minimum allowed photon energy width for a given pulse length, that is transform-limited pulses.

The self-seeding scheme is a promising approach to significantly narrow the SASE bandwidth and to produce nearly transform-limited pulses [4]-[20]. As shown in Fig. 1, the self-seeding setup consists of two undulators separated by a photon monochromator and an electron bypass beam line, normally a 4-dipole chicane. The two undulators are resonant to the same radiation wavelength. The SASE radiation generated by the first undulator passes through the narrow-band monochromator to create a transform-limited pulse, which is then used as a coherent seed in the second undulator. Chromatic dispersion effects in the bypass chicane smear out the microbunching in the electron bunch produced by the SASE lasing in the first undulator. The electrons and the monochromatized photon beam are recombined at the entrance of the second undulator, and the radiation is amplified by the electron bunch in the second undulator, until saturation is reached. The required seed power at the beginning of the second undulator must dominate over the shot noise power within the gain bandpass, which is order of a few kW.

For hard X-ray self-seeding, a monochromator is normally configured with

three undulator configuration

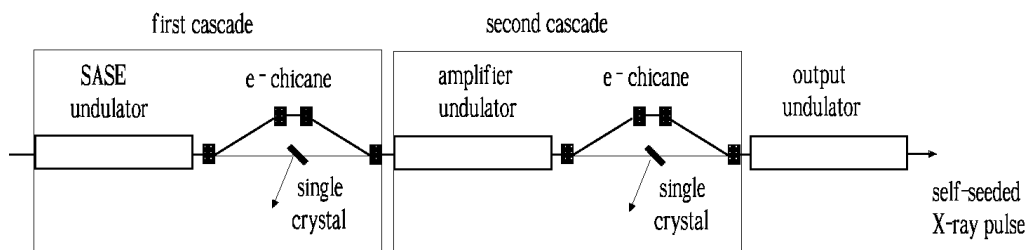


Fig. 2. Schematics of a two-cascade self-seeding scheme with single crystal monochromators. This amplification-monochromatization cascade scheme is distinguished, in performance, by a high spectral purity of the output radiation.

crystals in the Bragg geometry. A conventional 4-crystal monochromator introduces an optical delay at least a few millimeters, which has to be compensated with the introduction of a long electron bypass. To avoid such a long chicane, a simpler self-seeding scheme was proposed in [12]-[18], which uses the transmitted X-ray beam from a single crystal to seed the same bunch (see Fig. 1).

With radiation beam monochromatized down to the Fourier transform limit, a variety of very different techniques leading to further improvement of the X-ray FEL performance become feasible. Despite the unprecedented increase in peak power of the X-ray pulses for SASE X-ray FELs, some applications, including single biomolecule imaging, may require still higher photon flux. The most promising way to extract more FEL power than that at saturation is by tapering the magnetic field of the undulator [21]-[24]. Also, a significant increase in power is achievable by starting the FEL process from monochromatic seed rather than from noise [25]-[27]. Recently we proposed to make use of a single crystal self-seeding scheme to be installed in the tunable-gap baseline undulator at the European XFEL to create a source capable of delivering transform-limited X-ray pulses at extraordinary peak power level (0.4 TW) [14]. This single crystal self-seeding scheme was examined in [14] for the European XFEL by using ideal electron beam characteristics.

A typical X-ray FEL beam after acceleration and compression is usually not as simple as the case discussed in that paper, which deals with a Gaussian

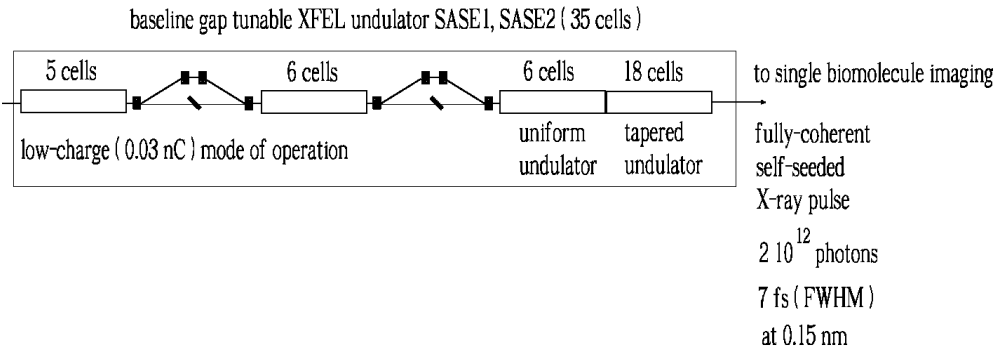
beam distribution and ignores wakefield effects. In the present paper we extend our consideration to a more realistic electron beam distribution at the undulator entrance. In particular, we propose a study of the performance of single-crystal self-seeding scheme for the European XFEL, based on start-to-end simulations, and accounting for undulator wakefields [28]. We optimize our self-seeding setup, based on the results of start-to-end simulations for an electron beam with 30 pC charge. Our analysis indicates that the self-seeding scheme is not significantly affected by non-ideal electron phase space distribution, and yields about the same performance as in the case for an electron beam with ideal properties. Simulations show that the FEL power of the transform-limited X-ray pulses may be increased up to 0.4 TW by operating with a tapered baseline undulator. In particular, it is possible to create a source capable of delivering fully-coherent, 7 fs (FWHM) X-ray pulses with  $2 \cdot 10^{12}$  photons per pulse at a wavelength of 0.15 nm.

## **2 Possible single-crystal self-seeding scheme for the European XFEL baseline undulator**

In its simplest configuration, a self-seeding FEL consists of an input and output undulator separated by a monochromator. With reference Fig. 2 we discuss the simplest two-undulator configuration case for the single-crystal self-seeding setup. The first undulator operates in the linear high-gain regime starting from the shot-noise in the electron beam. After the first undulator the output SASE radiation passes through the monochromator, which reduces the bandwidth. A distinguishing feature of our proposed setup is that it takes advantage of a single crystal in Bragg transmission geometry, instead of a fixed exit four-crystal monochromator. Due to nearly 100% in-band reflectivity, in the frequency domain the crystal works as a notch filter for the transmitted X-rays and generates a monochromatized wake in the time domain. The delay time of this monochromatized pulse from the main FEL pulse is determined by the width of the notch filter. The peak of the wake is about 10 MW and is delayed from the main SASE pulse by  $6 - 7 \mu\text{m}$ . A weak magnetic chicane (about 5 m long) is sufficient to delay the electron bunch and to smear out the SASE microbunching induced in the first part of the undulator. Since the rms electron bunch length is about  $1 \mu\text{m}$ , after the chicane the wake can be superimposed to the entire electron bunch, and acts as effective seed in the second undulator. In order for the seed to dominate the shot-noise generated in the second undulator, the SASE FEL in the first undulator has to provide sufficiently high FEL power to compensate for the power reduction associated with the passage through the single-crystal monochromator.

In some experimental situations, the simplest two-undulator configuration

combination of self-seeding scheme and tapering undulator technique would be of great importance especially for single biomolecule imaging



such very short and very intense single mode X-ray pulses may permit atomic resolution imaging of single macromolecule

Fig. 3. Design of an undulator system for high power mode of operation. The method exploits a combination of a cascade self-seeding scheme with single crystal monochromators and an undulator tapering technique. This scheme holds a great promise as a source of X-ray radiation for applications such as single biomolecule imaging.

is not optimal. For example, the European XFEL is characterized by a very high repetition rate, and a peculiar bunch structure, leading to important heat-loading of the monochromator and limiting the maximal seed power from the first undulator part. A possible extension of the two-undulator configuration consists in a setup with three undulators separated by monochromators, Fig. 2. This amplification-monochromatization cascade scheme is distinguished, in performance, by high spectral purity of the output radiation and a small heat-loading of the monochromator crystals.

Finally, the most promising way to increase the output power of the X-ray FEL is by tapering the magnetic field of the undulator. Tapering consists in a slow reduction of the field strength of the undulator in order to preserve the resonance wavelength, while the kinetic energy of the electrons decreases due to the FEL process. The undulator taper could be simply implemented as a step taper from one undulator segment to the next. The magnetic field tapering is provided by changing the undulator gap. A further increase in power is achievable by starting the FEL process from the monochromatic seed, rather than from noise. The reason is the higher degree of coherence of the radiation in the seed case, thus involving, with tapering, a larger portion of the bunch in the energy-wavelength synchronism.

Here we study a scheme for generating TW-level X-ray pulses in a tapered undulator with the use of cascade self-seeding technique for highly

monochromatic seed generation. In this way the output power of European X-ray FEL could be increased from baseline value of 20 GW to about 400 GW at 0.15 nm wavelength. Fig. 3 shows the design principle of our setup for high power mode of operation. The scheme consists of two parts: a succession of two amplification-monochromatization cascades and an output undulator in which the monochromatic seed signal is amplified up to the TW power-level. Each cascade consists of an undulator, acting as an amplifier, and a monochromator. Calculations show that in order not to spoil the electron beam quality and to simultaneously solve the heat-loading problem for the monochromator, the number of cells in the first and second cascade should be 5 and 6 respectively. The output undulator consists of two sections. The first section is composed by an uniform undulator, the second section by a tapered undulator. In the two cascades a nearly transform-limited FEL pulse is produced, which is then exponentially amplified passing through the first uniform part of the output undulator. This section is long enough (6 cells) to reach saturation, which yields about 20 GW power. Finally, in the second part of the output undulator the monochromatic FEL output is enhanced up to 400 GW with a 2% taper of the undulator parameter over the last 18 cells after saturation.

For the European XFEL, our cascade scheme trivially satisfies heat loading restrictions for the average power density, where the situation is indeed much better than at third generation synchrotron radiation sources. The energy per bunch impinging on the second crystal, which bears the largest heat-load, can be estimated as  $3\mu\text{J}$  (see section 3). One can easily estimate an average power of 0.1 W ( $3\mu\text{J}$  times 2700 pulses per train times 10 trains/s). We consider a transverse rms dimension of the bunch of about  $15\mu\text{m}$ . Within a short (5 m -long) magnetic chicane, the divergence of the X-ray radiation pulse is negligible, and the radiation power is distributed as the electron bunch. As a result we obtain illuminated crystal area of  $1.2 \cdot 10^{-3}\text{ mm}^2$ . This corresponds to a normal incident power density of about  $100\text{W}/\text{mm}^2$  at the position of the second monochromator, about an order of magnitude smaller compared to the average power density at monochromators of third generation synchrotron sources.

However, the European XFEL differs compared to third generation sources in the very specific time diagram, which foresees the production of about 10 trains of pulses per second, each train consisting of 2700 pulses. In this case, the average power density along a single pulse train is the meaningful figure of merit, rather than the above-mentioned average power density. The average power within a single bunch train can be estimated by multiplying the energy by about 3000 pulses composing a single train and dividing by a temporal duration of a train, which is 0.6 ms. One obtains power of 20 W. Considering illuminated area as  $10^{-3}\text{ mm}^2$ , as before, we obtain a power density of about  $10\text{kW}/\text{mm}^2$  within a single train, at normal incidence.

Table 1

Parameters for the low-charge mode of operation at the European XFEL used in this paper.

	Units	
Undulator period	mm	40
Periods per cell	-	125
K parameter (rms)	-	2.15
Total number of cells	-	35
Intersection length	m	1.1
Wavelength	nm	0.15
Energy	GeV	14.0
Charge	pC	28

Such heat-load is an order of magnitude smaller than what is foreseen at monochromators for the SASE2 baseline, where a diamond crystal with the same thickness (0.1 mm) is planned to be used.

### 3 Simulations

#### 3.1 Start-to-end electron beam simulations

In this Section we report on a feasibility study performed with the help of the FEL code GENESIS 1.3 [29] running on a parallel machine. We will present a feasibility study for a short-pulse mode of operation of the SASE1 and SASE2 FEL lines of the European XFEL, based on a statistical analysis consisting of 100 runs. The overall beam parameters used in the simulations are presented in Table 1. We refer to the setup in Fig. 3.

The expected beam parameters at the entrance of the SASE1 and SASE2 undulators are shown in Fig. 4, [28]. Wakes inside the undulators are also accounted for and expected to obey the dependence in Fig. 5, [28].

The evolution of the rms horizontal and vertical beamsizes as a function of the distance along the setup can be calculated through Genesis, and is shown in Fig. 6. The figure shows the evolution for the position of maximal current in the bunch, where normalized horizontal and vertical emittances are, respectively,  $\varepsilon_x = 1.37 \cdot 10^{-7}$  m and  $\varepsilon_y = 2.4 \cdot 10^{-7}$  m. Inspection of Fig. 6 shows a little mismatch in the vertical direction  $y$ , which is not present in the horizontal direction, and is due to the fact that undulator focusing forces



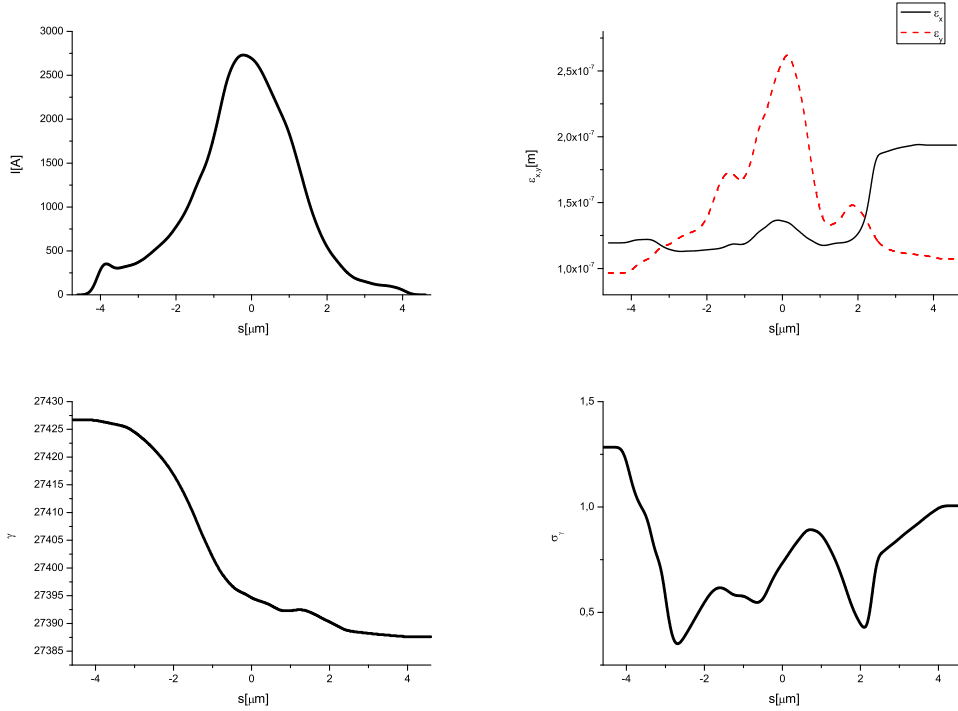


Fig. 4. Results from electron beam start-to-end simulations at the entrance of SASE1 and SASE2 [28]. (Top Left) Current profile. (Top Right) Normalized emittance as a function of the position inside the electron beam. (Bottom Left) Energy profile along the beam. (Bottom right) Electron beam energy spread profile.

are in the vertical direction only. The mismatch is automatically accounted for in the Genesis simulations. Since it turns out to be not significant, we keep a uniform FODO lattice focusing system.

### 3.2 SASE radiator and first crystal monochromator

According to the scheme in Fig. 3, the electron beam first goes through 5 undulator cells radiating in the SASE mode. The power and spectrum from the SASE radiator are shown in Fig. 7.

After the first undulator, the output SASE radiation passes through the monochromator, consisting of a crystals in the Bragg transmission geometry, Fig. 2. The crystal operates as bandstop filters for the transmitted X-ray SASE radiation pulse, Fig. 8, left plot. The modulus and the phase of the transmissivity is calculated with the help of the dynamical theory of X-ray diffraction. The output spectrum is given by the product of  $|T|^2$  with the initial SASE spectrum in Fig. 7, and is shown in Fig. 9, right plot. The temporal waveform of the transmitted radiation pulse shows a long tail, shown in Fig. 9, right plot, which can be used for seeding the electron bunch after

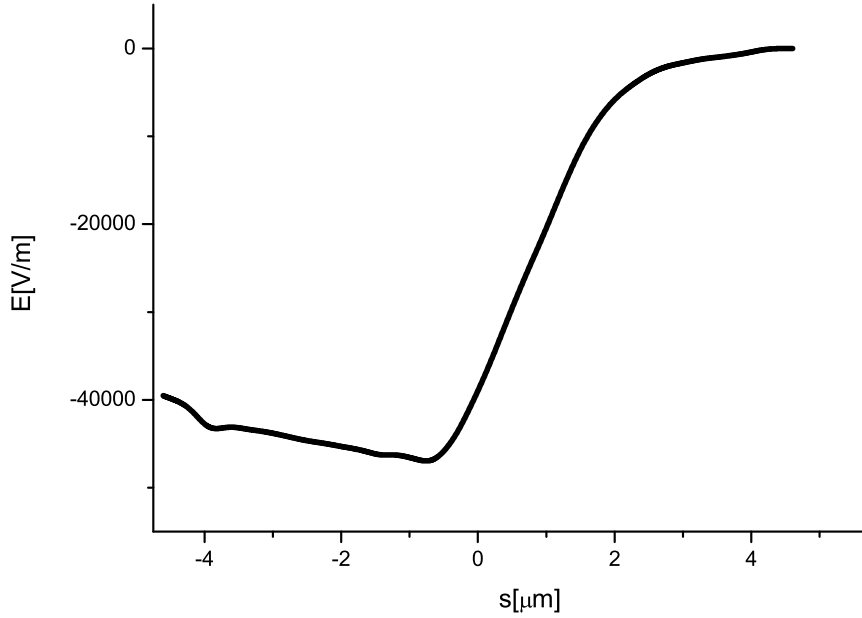


Fig. 5. Resistive wakefields in the SASE 1 (SASE 2) undulator [28]

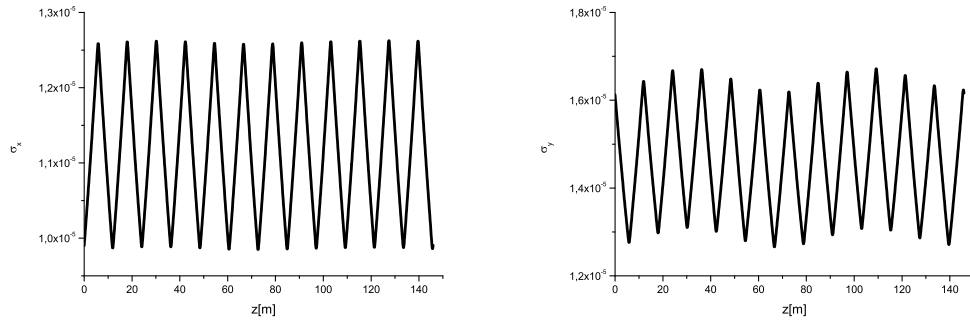


Fig. 6. Evolution of the rms horizontal (left plot) and vertical (right plot) beam size as a function of the distance along the setup calculated through GENESIS. These plots refer to the position within the bunch where the current is maximal. The normalized horizontal emittance is  $\varepsilon_x = 1.37 \cdot 10^{-7}$  m. The normalized vertical emittance is  $\varepsilon_y = 2.4 \cdot 10^{-7}$  m.

the chicane. The presence of such tail can be seen as a direct consequence of the Fourier transform relations. In particular, the Fourier transform of the transmissivity is shown in Fig. 8, right plot. The modulus of the Fourier transform of  $T$  exhibits oscillations which are inversely proportional to the bandwidth of the absorption line in the transmittance spectrum. This is easy to explain in terms of the Fourier transform of a square function. The sharp peak at  $s = 0$  corresponds to the long, nearly constant ends of  $|T|$  at large and small frequencies, which can be seen in Fig. 8, left plot. Finally, the presence

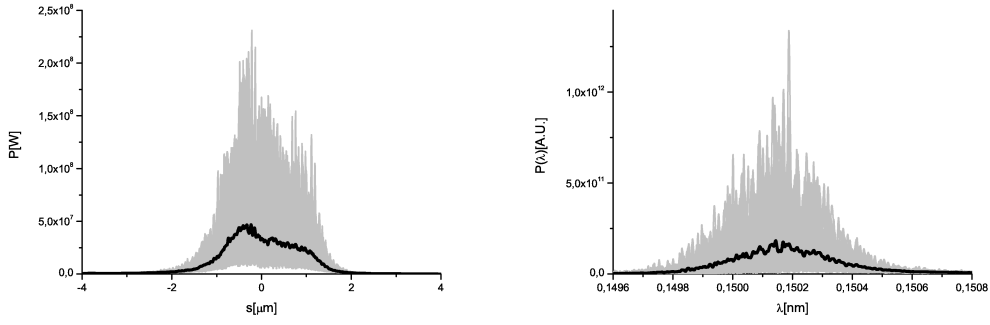


Fig. 7. (Left plot) SASE input power before the first crystal. (Right plot) SASE input spectrum before the first crystal. Grey lines refer to single shot realizations, the black line refers to the average over a hundred realizations.

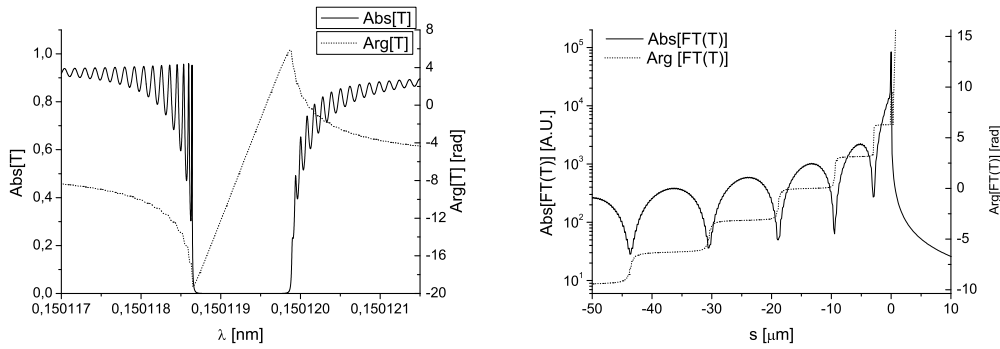


Fig. 8. (Left plot) Transmissivity (sigma polarization) relevant to the Bragg 400 diffraction of X-rays at 0.15 nm from a Diamond crystal with a thickness of 0.1mm. (Right plot) Fourier Transform of the transmissivity in the left plot.

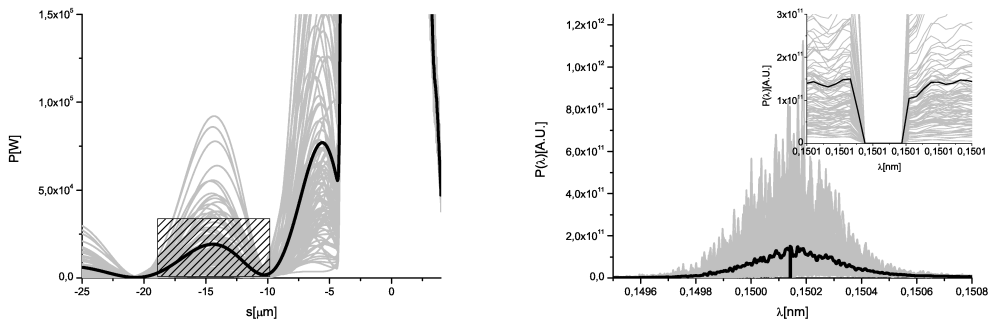


Fig. 9. (Left plot) Seed power after the first crystal. (Right plot) The effect of the first crystal on the SASE spectrum. Grey lines refer to single shot realizations, the black line refers to the average over a hundred realizations.

of a particular phase in  $T$  is related with the fulfillment of the causality requirement, so that the modulus of the Fourier transform of  $T$  vanishes at positive values of  $s$ .

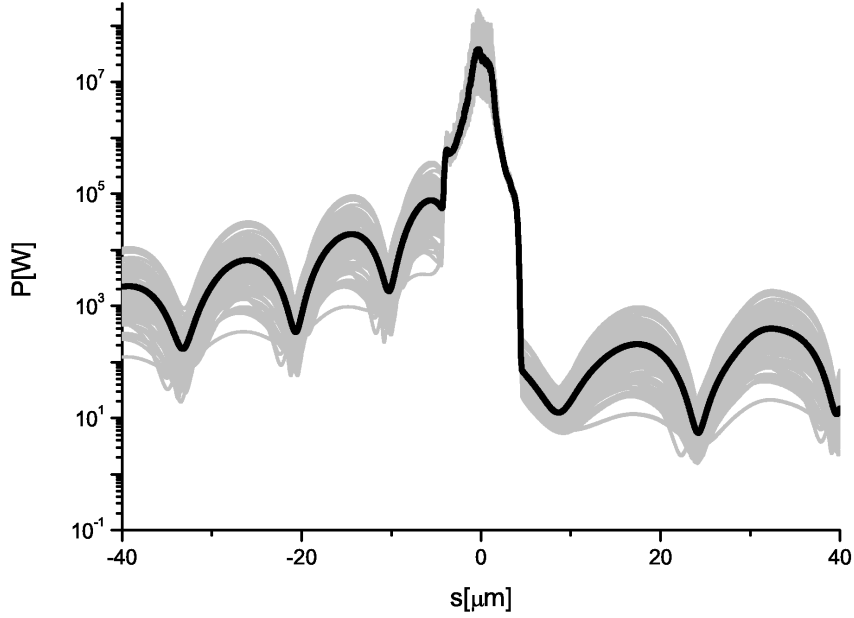


Fig. 10. Logarithmic plot of the seed power after the first crystal. Grey lines refer to single shot realizations, the black line refers to the average over a hundred realizations.

The temporal wavefront of the transmitted radiation is obtained convolving Fig. 8, right plot, with the SASE field in the time domain. In other words, the Fourier transform of the transmissivity can be seen as the input response of a filter. Since we consider the low charge mode of operation, the oscillations of the modulus of the Fourier transform of  $T$  extend for a length which is greater than the bunch length, so that the length of the oscillations in Fig. 9, right plot, are nearly inversely proportional to the bandwidth of the absorption line in the transmittance spectrum, as those in Fig. 8, left plot, as it can be seen by comparing that plot with Fig. 10. Very small but visible departure from the zero power level (the theoretical value due to causality) appears in the right-hand side of Fig. 10, for  $s > 0$ . This accuracy is acceptable for most purposes.

It is interesting to study the phase of the field after seeding, and to discuss possible phase effects due to the Diamond crystal. One can see from Fig. 8, right plot, that the phase introduced by the crystal is almost flat around the maxima of a given oscillation, and it varies only of a fraction of a radian around the seeding area in the low charge mode of operation<sup>2</sup>. This allows

<sup>2</sup> In the long bunch mode of operation, variation in phase is much more important, in the order of 10 rad, but still around the value  $2\pi$ , which allows for nearly Fourier limited pulses.

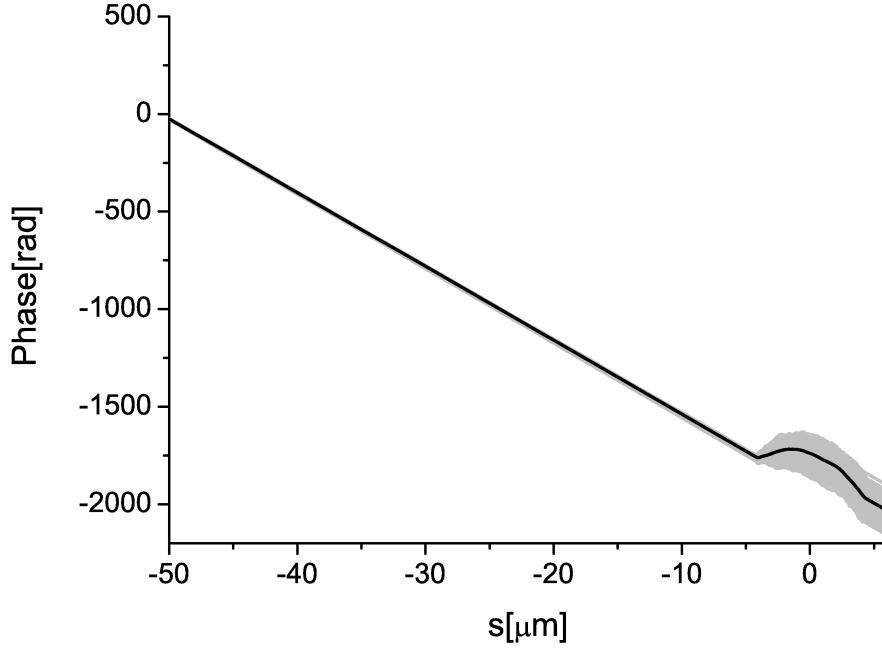


Fig. 11. Phase relation along the FEL pulse after the first crystal. The large linear chirp is due to the definition of the reference carrier frequency by Genesis, and is artificial. Grey lines refer to single shot realizations, the black line refers to the average over a hundred realizations.

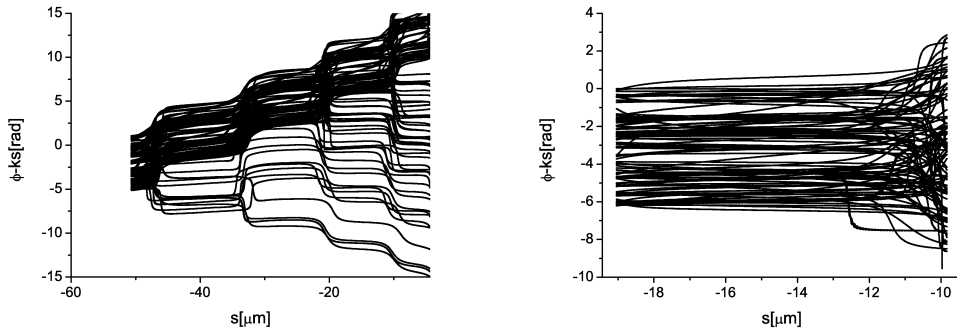


Fig. 12. (Left plot) Phase relation along the FEL pulse after the first crystal. The artificial, linear chirp has been subtracted. (Right plot) An enlargement of the left plot. One hundred single-shot realizations are shown in the plots.

for nearly Fourier limited pulses, which are characterized by the smallest possible time-bandwidth product. We checked that this property is inherited by the electric field after the crystal. Fig. 11 shows the phase after the crystal as a function of the position inside the FEL pulse. The large linear chirp in the seeding part is due to the definition of the reference carrier frequency by Genesis, which coincides with the resonant frequency of the undulator. Since the bandstop is shifted with respect to this reference carrier, a large,

artificial linear chirp is included by Genesis, which can be removed with appropriate subtraction. Fig. 12 shows the phase relation along the FEL pulse after subtraction of the linear chirp. The phase of the field varies well below a radian, and is consistent with the analysis of Fig. 8.

While the radiation is sent through the crystals, the electron beam passes through a magnetic chicane, which accomplishes three tasks: it creates an offset for the crystals installation, it removes the electron microbunching produced in the first undulator, and it acts as a delay line for the implementation of a temporal windowing process. In this process, the magnetic chicane shifts the electron bunch on top of the monochromatic tail created by the bandstop filter thus temporally selecting a part of it (see the highlighted area in Fig. 9, right plot). By this, the electron bunch is seeded with a radiation pulse characterized by a bandwidth much narrower than the natural FEL bandwidth. For the hard X-ray wavelength range, a small dispersive strength  $R_{56}$  in the order of a few microns is sufficient to remove the microbunching generated in the first undulator part. As a result, the choice of the strength of the magnetic chicane only depends on the delay that one wants to introduce between electron bunch and radiation. The optimal value amounts to  $R_{56} \approx 12 \mu\text{m}$  for the low-charge mode of operation. Such dispersion strength is small enough to be generated by a short (5 m-long) magnetic chicane to be installed in place of a single undulator module. Such chicane is, at the same time, strong enough to create a sufficiently large transverse offset for installing the crystal.

### 3.3 *Second radiator and second crystal*

The seed signal is amplified in the second undulator, Fig. 2, and filtered again. The input pulse impinging on the second crystal is shown in Fig. 13 in terms of power (left plot) and spectrum (right plot).

As discussed above, due to the shortness of the first undulator, the signal-to-noise ratio at the entrance of the second undulator cannot be much larger than unity. Nevertheless, as shown in [13] the monochromatic field amplitude at the entrance of the third undulator will be much larger than that at the entrance of the second.

In fact, the seed pulse after the second crystal is characterized in power and spectrum in Fig. 14. By inspection, the reader can conclude that the average seed power at the entrance of the output undulator is about 2 MW, while the effective shot noise power is about 3 kW. A comparison with the first cascade shows that the effective shot noise power is the same, but the monochromatic seed power is significantly smaller i.e signal to noise ratio at

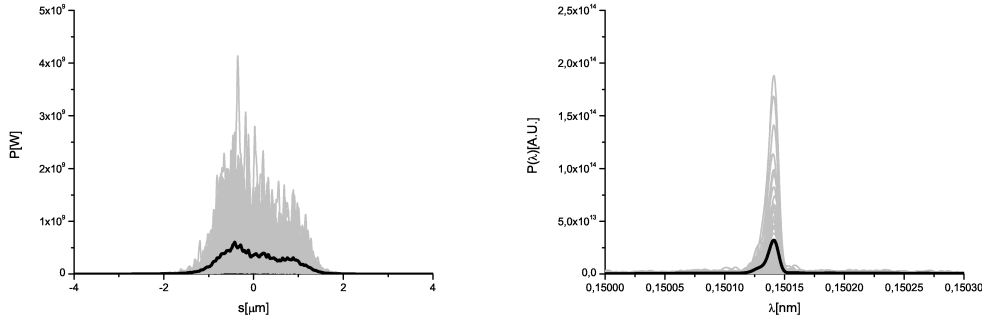


Fig. 13. (Left plot) Input power before the second crystal. (Right plot) Input spectrum before the second crystal. Grey lines refer to single shot realizations, the black line refers to the average over a hundred realizations.

the entrance of output undulator is much larger in the case of two cascades. compare with the case of one amplification-monochromatization cascade. This fact can be qualitatively explained as follows.

After amplification in the second undulator (Fig. 13), the bandwidth of the FEL pulse related with the monochromatic signal that impinges on the second crystal is near to the transform-limited bandwidth of the electron bunch i.e.  $c/\sigma_e$ . As a result, assuming the same amplification in the two cascades, the signal to noise ratio is enhanced by a factor  $\sigma_e \Delta\omega_{SASE}/c$ , where  $\Delta\omega_{SASE}$  is the SASE bandwidth. A rough estimate for the signal to noise ratio at the entrance of the third (output) undulator is therefore<sup>3</sup>  $P_{seed2}/P_n \sim (P_{seed1}/P_n)\sigma_e \Delta\omega_{SASE}/c \gg 1$ . Since this value is much larger than unity, we conclude that a double cascade self-seeding scheme using a single-crystal monochromator is insensitive to noise and non-ideal effects.

### 3.4 Output characteristics

After the seed leaves the second crystal, it is superimposed to the electrons at the entrance of the last undulator, where it is amplified up to saturation, Fig. 15. One finds an almost bandwidth-limited output pulse, i.e. a pulse with no frequency modulation. The output power is in excess of 20 GW,

<sup>3</sup> From our reasoning we conclude that the enhance of the signal-to-noise ratio is about a factor 100. This is the result of two effect. the first is the before-mentioned amplification of the monochromatic seed in the first cascade i.e.  $\sigma_e \Delta\omega_{SASE} \sim 10$ . The second reason is the presence of an extra cell in the second cascade, which additionally enhance the signal-to-noise ratio of a factor  $\sim 10$ . Of course, a configuration with 6 cells followed by 5 cells will lead to the same monochromatic seed at the entrance of the output undulator as the configuration with 5 cells followed by 6 cells.

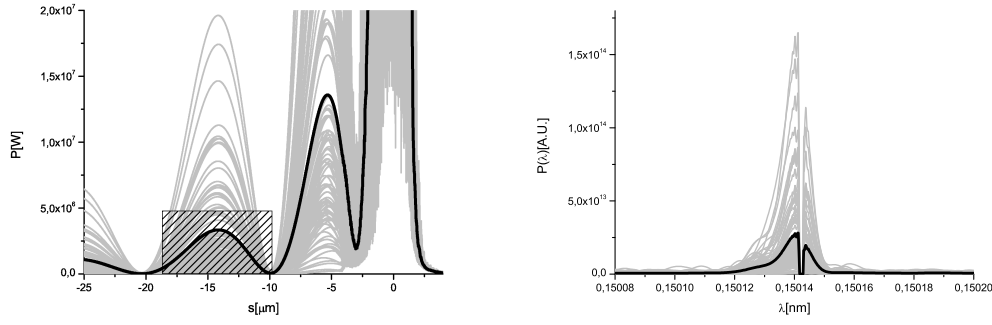


Fig. 14. (Left plot) Seed power after the second crystal. (Right plot) The effect of the second crystal on the input spectrum. Grey lines refer to single shot realizations, the black line refers to the average over a hundred realizations.

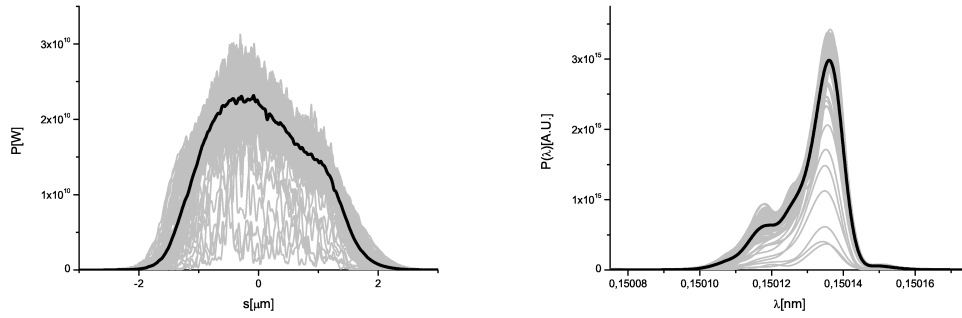


Fig. 15. Power distribution and spectrum of the X-ray radiation pulse at saturation without tapering. Here the output undulator is 7 cells long. Grey lines refer to single shot realizations, the black line refers to the average over a hundred realizations.

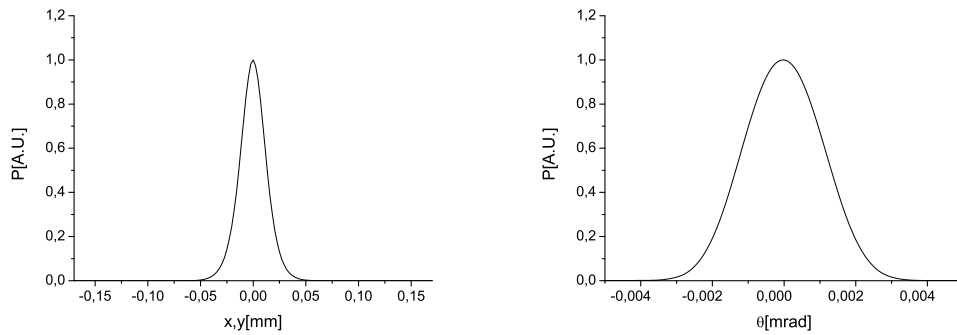


Fig. 16. (Left plot) Transverse radiation distribution at saturation without tapering at the exit of the output undulator. (Right plot) Directivity diagram of the radiation distribution at saturation without tapering at the exit of the output undulator.

and the nearly Fourier-limited bandwidth corresponds to a time-bandwidth product  $\Delta t \cdot \Delta\omega \simeq 6.6$ , to be compared with the minimal time-bandwidth



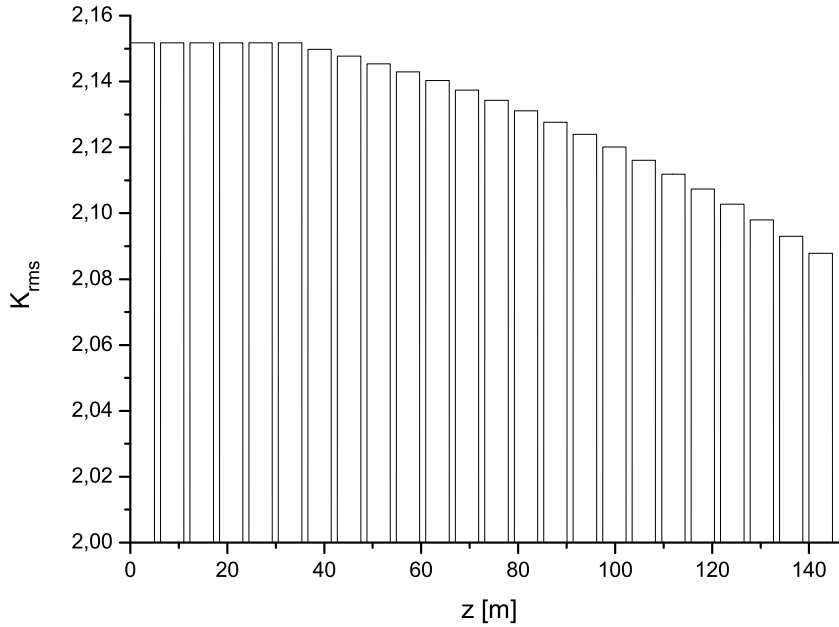


Fig. 17. Taper configuration for high-power mode of operation at 0.15 nm.

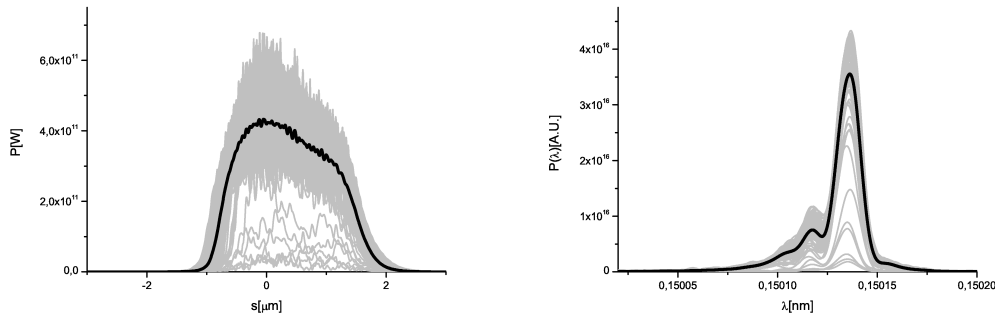


Fig. 18. (Left plot) Output power at saturation in the case of tapering. (Right plot) Output spectrum at saturation in the case of tapering. Grey lines refer to single shot realizations, the black line refers to the average over a hundred realizations.

product for a Gaussian<sup>4</sup> given by 2.8. The transverse radiation distribution and divergence at the exit of the output undulator are shown in Fig. 16.

<sup>4</sup> The time-bandwidth product constitutes a figure of merit for qualitative analysis only. In fact, in our case the time-domain pulse is non-Gaussian and non-symmetric. The time-bandwidth limit for a stepped-profile pulse is, for example, about 1.35 times larger than that for a Gaussian pulse. The comparison with the Gaussian case qualitatively shows that we are not far from the ultimate time-bandwidth product, and the difference can be explained, at least partially, by the asymmetry of the pulse profile in the time domain.

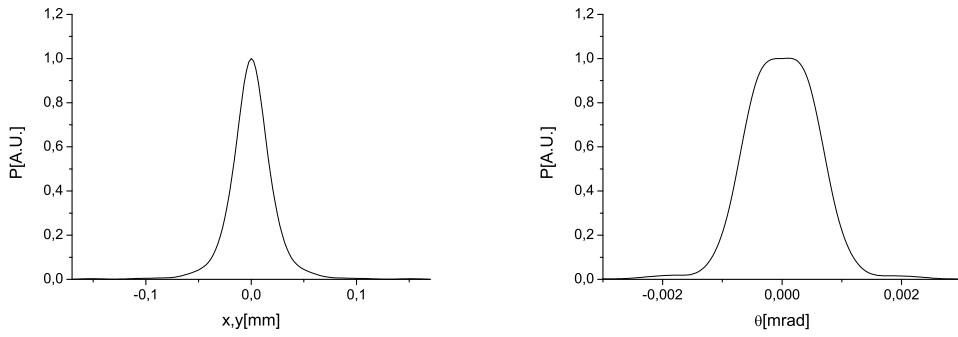


Fig. 19. (Left plot) Transverse radiation distribution in the case of tapering at the exit of the output undulator. (Right plot) Directivity diagram of the radiation distribution in the case of tapering at the exit of the output undulator.

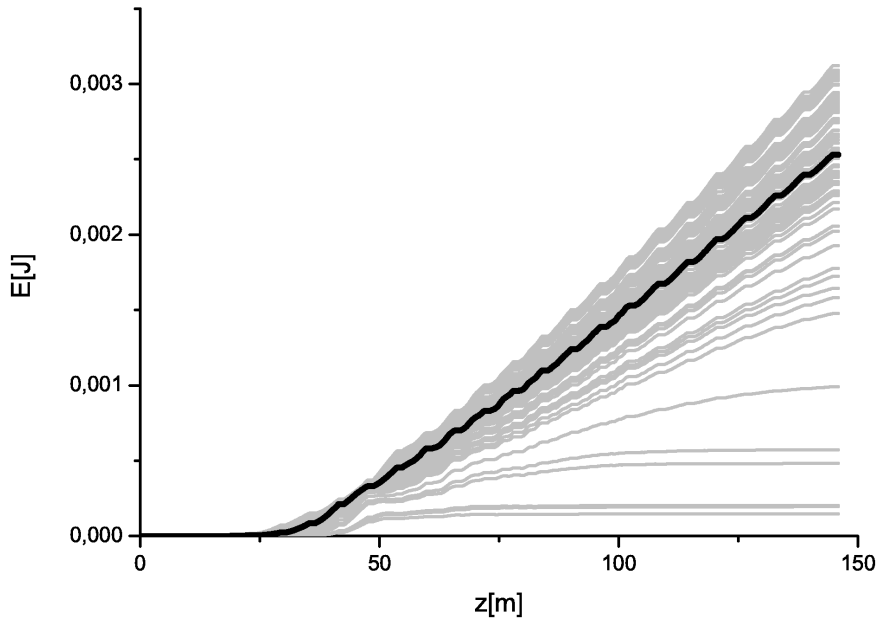


Fig. 20. Energy in the X-ray radiation pulse versus the length of the output undulator. Tapering is considered according to the law in Fig. 17. Grey lines refer to single shot realizations, the black line refers to the average over a hundred realizations.

One can prolong the exchange of energy to the photon beam by tapering the last part of the radiator on a segment-to-segment basis. The optimal tapering law is found empirically and is shown<sup>5</sup> in Fig. 17. Taper begins from the first

<sup>5</sup> Note that additional tapering should be considered to keep the undulator tuned in the presence of energy loss from spontaneous radiation. In Fig. 17 we present a tapering configuration which is to be considered as an addition to this energy-loss compensation tapering.

six cells. The output power and spectra at the exit of the setup are shown in Fig. 18. A final output power in the TW level (400 GW) can be reached with the help of the baseline undulator, while the radiation pulse remains nearly Fourier limited, with a time-bandwidth product  $\Delta t \cdot \Delta\omega \simeq 8.0$ . The transverse radiation distribution and divergence at the exit of the output undulator are shown in Fig. 19. The evolution of the energy in the radiation pulse as a function of the output undulator length is shown in Fig. 20.

To conclude, it is interesting to compare our previous calculations for the European XFEL [14] with the ones discussed in the present article. In fact, in this work we make use of the phase space distribution from start-to-end simulations, we include wakes and, additionally, we reduced the energy of electron beam (of 3.5 GeV) and shortened the undulator length (of 7 cells). The undulator period is also slightly different (40 mm, compared with 48 mm in the previous study). As a result of these changes, at first glance we should expect some performance degradation. The simulation results presented in this section show that this is not the case. The reduction of energy and undulator length can only lead to performance degradation. Similar reasoning holds for the presence of wakes. However, performance improvement is to be expected due to a better slice emittance. In previous calculations we considered  $0.4 \mu\text{m}$ , uniformly distributed normalized emittance based on the experience of the LCLS. In the present article, based on start to end simulations for the European XFEL we consider a slice emittance approximately two times smaller ( $< 0.25 \mu\text{m}$ ) within all bunch length for both directions (see Fig. 4). As our simulations have shown, this leads to performance increase and compensates for detrimental factors.

## 4 Conclusions

In the baseline SASE mode, the European XFEL will provide transversely coherent beams but only limited longitudinal coherence. However, an important goal for advanced XFEL sources is the creation of transform-limited pulses of radiation, which are important for several reasons. First, they naturally provide the maximum intensity within the minimum photon energy window for given pulse length, so that no monochromator is needed in the experimental hall or at the photon beam lines. Second, when the radiation beam is monochromatized down to the Fourier transform limit, a variety of very different techniques become feasible, leading to further improvement of the XFEL performance. For example, as we demonstrated in [14] for an ideal electron beam, monochromatization effectively allows one to use an undulator tapering technique enabling a high power mode of operation. Such mode of operation is highly desirable. In fact, in spite of the unprecedented increase in peak power of X-ray pulses from SASE XFELs, compared

with third generation facilities, some applications require still higher photon flux. In the present paper we extend our consideration to a realistic electron beam distribution at the undulator entrance. In particular we propose a study of the performance of a cascade self-seeding scheme with single crystal monochromators for European XFEL, based on start-to-end simulations and accounting for undulator wakefields [28]. By combining the two techniques of cascade self-seeding and undulator tapering, we find that TW-level X-ray pulses can be generated with minimal modifications to the baseline mode of operation. The results of our analysis indicate that our self-seeding scheme is not significantly affected by non-ideal electron phase space distribution and has about the same performance in the start to end case as for the electron beam with ideal properties.

## 5 Acknowledgements

We are grateful to Massimo Altarelli, Reinhard Brinkmann, Serguei Molodtsov and Edgar Weckert for their support and their interest during the compilation of this work.

## References

- [1] P. Emma et al., *Nature photonics* doi:10.1038/nphoton.2010.176 (2010)
- [2] T. Tanaka et al. (Eds.) *Spring-8 Compact SASE Source Conceptual Design report*, Kouto (2005) (See also <http://www-xfel.spring8.or.jp/SCSSCDR.pdf>)
- [3] M. Altarelli, et al. (Eds.) *XFEL, The European X-ray Free-Electron Laser, Technical Design Report*, DESY 2006-097, Hamburg (2006).
- [4] J. Feldhaus et al., *Optics. Comm.* 140, 341 (1997).
- [6] E. Saldin, E. Schneidmiller, Yu. Shvyd'ko and M. Yurkov, *NIM A* 475 357 (2001).
- [6] E. Saldin, E. Schneidmiller, Yu. Shvyd'ko and M. Yurkov, *NIM A* 475 357 (2001).
- [7] E. Saldin, E. Schneidmiller and M. Yurkov, *NIM A* 445 178 (2000).
- [8] R. Treusch, W. Brefeld, J. Feldhaus and U Hahn, *Ann. report 2001 "The seeding project for the FEL in TTF phase II"* (2001).
- [9] A. Marinelli et al., *Comparison of HGHG and Self Seeded Scheme for the Production of Narrow Bandwidth FEL Radiation*, *Proceedings of FEL 2008, MOPPH009*, Gyeongju (2008).
- [10] G. Geloni, V. Kocharyan and E. Saldin, "Scheme for generation of highly monochromatic X-rays from a baseline XFEL undulator", *DESY 10-033* (2010).

- [11] Y. Ding, Z. Huang and R. Ruth, *Phys.Rev.ST Accel.Beams*, vol. 13, p. 060703 (2010).
- [12] G. Geloni, V. Kocharyan and E. Saldin, "A simple method for controlling the line width of SASE X-ray FELs", DESY 10-053 (2010).
- [13] G. Geloni, V. Kocharyan and E. Saldin, "A Cascade self-seeding scheme with wake monochromator for narrow-bandwidth X-ray FELs", DESY 10-080 (2010).
- [14] G. Geloni, V. Kocharyan and E. Saldin, "Scheme for generation of fully coherent, TW power level hard x-ray pulses from baseline undulators at the European XFEL", DESY 10-108 (2010).
- [15] Geloni, G., Kocharyan, V., and Saldin, E., "Cost-effective way to enhance the capabilities of the LCLS baseline", DESY 10-133 (2010).
- [16] Geloni, G., Kocharyan, V., and Saldin, E., "Way to increase the user access at the LCLS baseline", DESY 10-165 (2010).
- [17] Geloni, G., Kocharyan V., and Saldin, E., "A novel Self-seeding scheme for hard X-ray FELs", *Journal of Modern Optics*, DOI:10.1080/09500340.2011.586473
- [18] Geloni, G., Kocharyan V., and Saldin, E., "Generation of doublet spectral lines at self-seeded X-ray FELs", DESY 10-199 (2010), and *Optics Communications*, 284, 13, 3348 (2011)
- [19] W.M. Fawley et al., Toward TW-level LCLS radiation pulses, TUOA4, to appear in the FEL 2011 Conference proceedings, Shanghai, China, 2011
- [20] J. Wu et al., Simulation of the Hard X-ray Self-seeding FEL at LCLS, MOPB09, to appear in the FEL 2011 Conference proceedings, Shanghai, China, 2011
- [21] A. Lin and J.M. Dawson, *Phys. Rev. Lett.* 42 2172 (1986)
- [22] P. Sprangle, C.M. Tang and W.M. Manheimer, *Phys. Rev. Lett.* 43 1932 (1979)
- [23] N.M. Kroll, P. Morton and M.N. Rosenbluth, *IEEE J. Quantum Electron.*, QE-17, 1436 (1981)
- [24] T.J. Orzechowski et al., *Phys. Rev. Lett.* 57, 2172 (1986)
- [25] W. Fawley et al., *NIM A* 483 (2002) p 537
- [26] M. Cornacchia et al., *J. Synchrotron rad.* (2004) 11, 227-238
- [27] X. Wang et al., *PRL* 103, 154801 (2009)
- [28] I. Zagorodnov, Private communication
- [29] S Reiche et al., *Nucl. Instr. and Meth. A* 429, 243 (1999).